Electronic structure and spin-orbit driven novel magnetism in $d^{4.5}$ insulator $Ba_3YIr_2O_9$

S. K. Panda,[1,*] S. Bhowal,[2] Ying Li,[3] S. Ganguly,[2] Roser Valentí,[3] L. Nordström,[4] and I. Dasgupta[1,2,†]

[1] *Centre for Advanced Materials, Indian Association for the Cultivation of Science, Jadavpur, Kolkata-700032, India*
[2] *Department of Solid State Physics, Indian Association for the Cultivation of Science, Jadavpur, Kolkata-700032, India*
[3] *Institut für Theoretische Physik, Goethe-Universität Frankfurt, Max-von-Laue-Strasse 1, 60438 Frankfurt am Main, Germany*
[4] *Department of Physics and Astronomy, Uppsala University, Box 516, SE-75120 Uppsala, Sweden*

arXiv:1511.03112v1 [cond-mat.str-el] 10 Nov 2015

We have carried out a detailed first-principles study of a $d^{4.5}$ quaternary iridate $Ba_3YIr_2O_9$ both in its 6H-perovskite-type ambient pressure (AP) phase and also for the high pressure (HP) cubic phase. Our analysis reveals that the AP phase belongs to the intermediate spin-orbit coupling (SOC) regime. This is further supported by the identification of the spin moment as the primary order parameter (POP) obtained from a magnetic multipolar analysis. The large t_{2g} band width renormalizes the strength of SOC and the Ir intersite exchange interaction dominates resulting in long range magnetic order in the AP phase. In addition to SOC and Hubbard U, strong intradimer coupling is found to be crucial for the realization of the insulating state. At high pressure (HP) the system undergoes a structural transformation to the disordered cubic phase. In sharp contrast to the AP phase, the calculated exchange interactions in the HP phase are found to be much weaker and SOC dominates leading to a quantum spin orbital liquid (SOL) state.

PACS numbers: 71.15.Mb 71.70.Ej 75.30.Et

The 5-d Ir based oxide systems have become very fascinating as they offer a novel ground for understanding the physics driven by the interplay between SOC, on-site Coulomb repulsion (U), crystal-field splitting, and intersite hopping. Many exotic phases like novel j_{eff}=$\frac{1}{2}$ Mott state, quantum spin liquid (QSL), topological insulator, and other emergent states have been realized in these systems[1–8]. Kim *et al.*[9,10] first reported spin-orbit driven Mott-insulating state in Sr_2IrO_4 where a large SOC (λ) further splits the t_{2g} orbitals of Ir^{4+} ($5d^5$) into a completely filled $j_{eff} = \frac{3}{2}$ and a half-filled $j_{eff} = \frac{1}{2}$ doublet which in the presence of relatively small value of U split into lower and upper Hubbard bands leading to a spin-orbit-driven Mott insulator. In this respect, the 6H perovskite type quaternary iridates $Ba_3MIr_2O_9$, where Ir ions form structural dimers, attracted considerable attention because a non magnetic M atom provides a knob to tailor the valence of Ir. Interestingly, Ir in oxidation state other than the usual 4+ (d^5) are not only insulating but also exhibit emergent phases like a spin-orbital liquid (SOL) state in $Ba_3ZnIr_2O_9$[11] and a pressure induced transition from long range order to spin liquid state in $Ba_3YIr_2O_9$[12]. The compound $Ba_3YIr_2O_9$ with fractional charge state $Ir^{4.5+}$ is intriguing on several counts. In the j_{eff}=$\frac{1}{2}$ picture the insulating state of $Ba_3YIr_2O_9$ is not obvious as Ir with 4.5 electrons is a quarter filled system as opposed to half filled d^5 iridates. The origin of pressure induced magnetic transition in this system has also remained unexplored. Further there could be a possibility of a temperature dependent structural transformation to a charge ordered (CO) state, as seen in $Ba_3NaRu_2O_9$[13].

Earlier experimental studies on $Ba_3YIr_2O_9$[14] at ambient pressure (AP) reported a sharp anomaly at 4 K in the heat capacity data although no such feature was seen in the susceptibility data. Later, Dey *et al.*[15] found that the variation of the susceptibility with temperature shows a weak anomaly at about 4 K in agreement with previous heat capacity measurements reflecting the presence of long-range ordering. The susceptibility data[15] follows a Curie-Weiss (CW) behavior with $\theta_{CW} \sim 0$ and effective moment 0.3 μ_B much less than the spin-only value expected for a $d^{4.5}$ system. On the other hand, the high-pressure (HP) synthesized sample undergoes a structural phase transition and does not order down to 2 K as evidenced from susceptibility, heat capacity, and nuclear magnetic resonance (NMR) measurements and is suggested to be a 5d-based, gapless QSL[12].

In view of the above, and also due to the fact that iridates, where Ir ions are in a fractional charge state and form structural dimers, have not been explored before, we have performed density functional theory (DFT) electronic structure calculations within the local density approximation (LDA) as well as LDA+U+SOC that includes the Hubbard U and SOC using the augmented plane waves plus local orbitals (APW + lo) method as implemented in the ELK code[1–3]. The SOC was treated through the second variational method. In this approach, given a value of U using a screened Coulomb potential (Yukawa potential) the corresponding onsite exchange energy J (Hund's coupling) is calculated[2]. The ELK code was also employed to identify the primary order parameter (POP) responsible for breaking of the time reversal (TR) symmetry. Calculations were also done within the generalized gradient approximation (GGA) [10] as well as GGA+U+SOC using the LAPW method as implemented in Wien2k[4] and also projector augmented wave (PAW) method as implemented in the Vienna *ab initio* simulation package (VASP)[5,6,11,12]. While these results are very similar to the LDA+U+SOC study, as expected, GGA systematically overestimated the magnitude of the

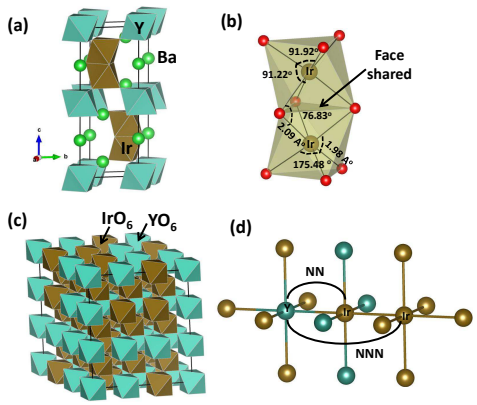

FIG. 1: (color online) (a) The crystal structure for the hexagonal AP phase of Ba_3YIrO_9. (b) Ir_2O_9 face-shared bioctahedra. (c) Crystal structure for the Cubic HP phase $Ba_2Ir(Y_{2/3}Ir_{1/3})O_6$. (d) In the HP phase, the nearest neighbor(NN) of Y is always Ir while the next nearest neighbor(NNN) of Y can be either Ir or Y due to disorder.

magnetic moment. In order to extract the tight binding parameters and to understand the crystal field splitting, we have constructed low energy model Hamiltonian using the downfolding procedure as implemented in the N^{th} order muffin-tin-orbital (NMTO) method[7–9] with self-consistent potentials obtained from linear muffin tin orbital (LMTO) calculations. The technical details of all the methods are discussed in Supplementary Materials (SM)[29].

At ambient pressure (AP), $Ba_3YIr_2O_9$ crystallizes in a 6H-perovskite-type structure[12] with space group $P6_3/mmc$ containing two formula units and hence two structural Ir dimers in the unit cell which are connected via O-Y-O paths along the c-axis [see Fig 1(a)]. As shown in Fig 1(b), each distorted IrO_6 octahedra share their face with the neighboring one, forming Ir_2O_9 face-shared bioctahedra. The high pressure (HP) phase of $Ba_3YIr_2O_9$, on the other hand crystallizes in the disordered cubic phase $Ba_2Ir(Y_{2/3}Ir_{1/3})O_6$ as shown in Fig. 1(c), where IrO_6 (brown) and YO_6 (cyan) octahedra are arranged, in such a way that each Y has 6 Ir as its NN but the NNN can be either Y or Ir [see Fig. 1(d)][12].

We have first investigated the electronic structure of the AP phase of $Ba_3YIr_2O_9$ without any magnetic order. The characteristic feature of the band structure (see Fig. 1 of SM) is the isolated manifold of twelve t_{2g} bands hosting the Fermi level (E_F) arising from the four Ir atoms in the unit cell and is well separated by a gap of 2.5 eV from another complex of eight e_g bands. The t_{2g}-e_g crystal field splitting ($\Delta_{t_{2g}-e_g}$) is large. The distortion of the IrO_6 octahedron further splits the t_{2g} states into singly degenerate a_1 and doubly degenerate e_1 states with the e_1 states lower in energy by $\Delta_{CF} = 0.16$ eV (see SM for details). The Ba-s and Y-d states are completely empty and hence lie above E_F while O-p states, admixed with Ir-d states, are mostly occupied consistent with the nominal ionic formula $Ba_3^{2+}Y^{3+}Ir_2^{4.5+}O_9^{2-}$ for the system. Due to the small Ir-Ir distance the direct hopping between the a_1 orbital (see SM) is appreciable (-573.9 meV) which is also reflected in the large t_{2g} band width ($\sim$ 1.88 eV) of $Ba_3YIr_2O_9$.

In order to understand the magnetic properties of the system four different magnetic configurations, namely FM (both the intra- and inter-dimer couplings are ferromagnetic), AFM1 (both the intra- and inter-dimer couplings are antiferromagnetic), AFM2 (intra-dimer coupling is ferromagnetic and inter-dimer coupling is antiferromagnetic), and AFM3 (intra-dimer coupling is antiferromagnetic and inter-dimer coupling is ferromagnetic) have been simulated (See Fig. 2 of SM). The results of our LDA+U+SOC calculation with $U = 4$ eV as obtained using the ELK code are shown in Fig 2(a). We observe that the AFM2 state has the lowest energy with the spin (orbital) moment on the Ir site to be 0.55 (0.34) μ_B. Spin and orbital moments are in the same direction as t_{2g} states are more than half filled. The relatively smaller value of $\frac{m_l}{m_s}$ ratio ($\sim$0.62) compared to the other SOC driven $j_{eff} = 1/2$ iridates, *i.e*, Sr_2IrO_4[9], (where it is $\sim$2) indicates the action of only moderately strong SOC in $Ba_3YIr_2O_9$. Fig. 2(a) also reveal that the magnitude of Ir magnetic moments fluctuate for parallel and antiparallel spin configurations in a dimer and only the AFM2 configuration is insulating as illustrated by the plot of band structure and DOS shown in Fig. 3(a) and 3(b) respectively. Although the LDA+U method is less accurate than, the LDA method for total energy calculations[30] and has a tendency to favor magnetism because of the additional effective Stoner coupling, it can still be used as a reference for magnetic states as discussed in Ref. 30. Therefore, a comparison of total energies among various magnetic configurations for $Ba_3YIr_2O_9$ should be reliable in a LDA+U+SOC calculation. The stability of the ferromagnetic (FM) arrangement of Ir atoms in a dimer in the AFM2 configuration indicates a strong influence of the effective Hund's coupling (J_H) in the system (which is directly related to the onsite exchange parameter J), pointing to the fact that J_H is not only larger than Δ_{CF} but also dominates over the splitting due to SOC (Δ_{SOC}). This hierarchy of energies helps to promote Ir-Ir double exchange. This is in contrast to $Ba_5AlIr_2O_{11}$[31], where SOC overcomes the Ir-Ir double exchange leading to an AFM arrangement of Ir spins in a dimer.

The origin of the insulating state in $Ba_3YIr_2O_9$ can be explained by the cooperative effect of J_H, Δ_{CF}, Δ_{SOC} and $t_{intra-dimer}$. In view of comparatively large J_H, we ignore the spin mixing term of the SOC Hamiltonian[32] and only concentrate on the minority t_{2g} bands. This simplification, allows us to diagonalise the SOC Hamiltonian, having matrix element $\langle i|\lambda\overline{L}\cdot\overline{S}|j\rangle$, (i,j = 1,2,3) and find that the degeneracy of $|1\rangle$ and $|2\rangle$ (i.e, e_1 orbitals) is lifted upon inclusion of SOC, while $|3\rangle$ (a_1 orbital) remains unperturbed [see inset of Fig. 3(b)]. In the presence of strong $t_{intra-dimer}$ (See

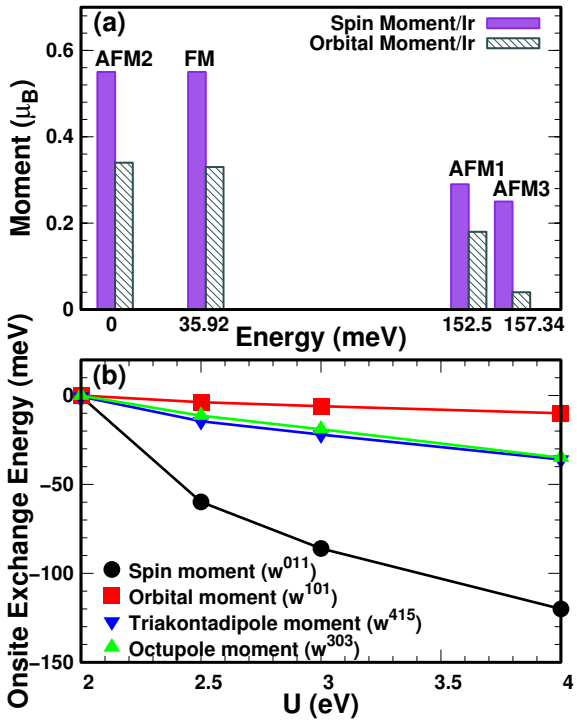

FIG. 2: (color online) (a) The variation of spin and orbital moment at the Ir site for various magnetic configurations in the AP phase. (b) Variation of onsite exchange energy associated with different order parameters (OP) with the variation of Hubbard U.

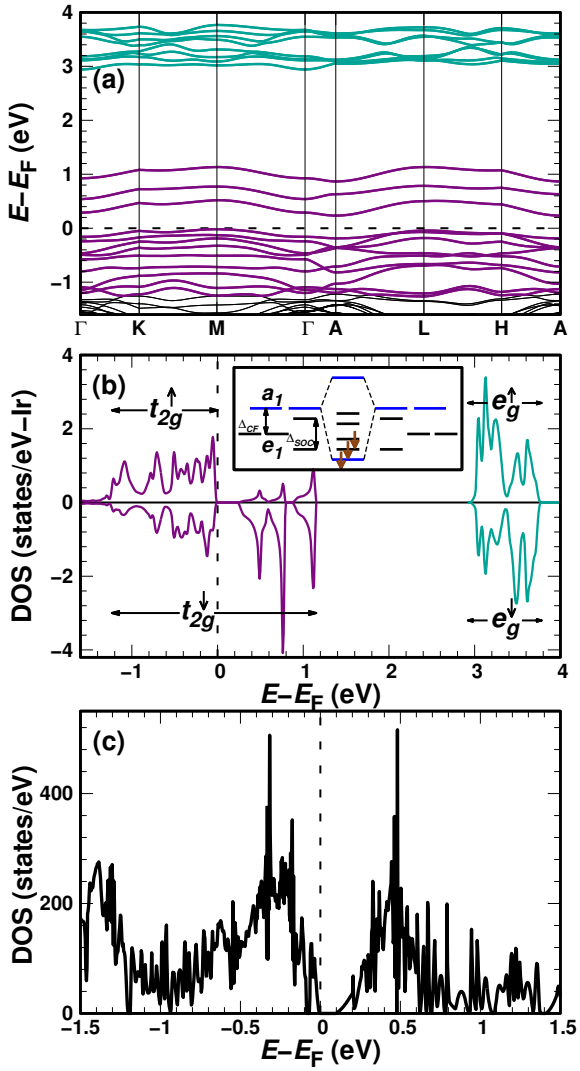

FIG. 3: (color online) (a) Bandstructure and (b) Partial density of states (DOS) for Ir-d projected onto up and down spin state for the AP phase. The inset shows the schematic diagram to explain the insulating behavior of AP phase. (c) The nonmagnetic DOS for the HP phase of Ba_3YIrO_9 in the presence of SOC and Hubbard U.

Table-I of SM), the states will interact strongly with each other and form six non-degenerate states. Three electrons available for a pair of Ir in a dimer in the minority spin channel will lead to an insulating state. Further inclusion of finite Hubbard U (4 eV), which is also crucial to stabilize magnetism, promotes an insulating state with an energy gap of 252 meV as shown in Fig. 3(b). The calculated total magnetic moment in the AFM2 phase is substantially higher from that expected for a quarter filled j_{eff}=1/2 system, indicating j_{eff}=1/2 model may not be relevant here.

The above discussion places $Ba_3YIr_2O_9$ in the intermediate SOC regime and may be attributed to the large t_{2g} band width that substantially renormalizes the strength of the atomic λ. In order to clarify this point further as well as to identify the order parameter (OP) responsible for breaking the time reversal (TR) symmetry that lead to magnetic order, we have carried out a multipolar (MP) analysis where the rotational invariant local Coulomb interaction is expanded in multipole tensors in the mean field limit. In the present case with Ir-d orbitals the density matrix D ($D = \langle d_n d_n^\dagger \rangle$, $d_n^\dagger$ and d_n being creation and annihilation vector operators respectively for d-states of Ir at site n) has 100 independent elements. This information carried by the density matrix can be transformed to expectation values of multipole tensor moments through $w^{kpr} = \mathrm{Tr}\,\Gamma^{kpr} D$, where the multipolar tensor operator Γ^{kpr} is an hermitian matrix-operator as given by Ref. 33 and the indices are determined through the coupling of angular momenta, $0 \le k \le 2\ell = 4$, $0 \le p \le 2s = 1$ and $|k-p| \le r \le |k+p|$. Altogether there are 18 different multipole tensors (which in total has 100 independent tensor components), of which 9 multipole tensors break the TR symmetry.

In terms of these moments, w^{kpr} the onsite exchange energy for the corresponding state (E_x) can be expanded as[34],

$$E_x = \frac{1}{2} \sum_{kpr} K_{kpr} w^{kpr} \cdot w^{kpr} \qquad (1)$$

where, K_{kpr} are the corresponding exchange parameters[2]. Thus the exchange energy (on site) associated with a multipole moment w^{kpr} can be identified[35]. This corresponds to the stabilization of the concerned multipolar

TABLE I: Energy difference between FM and two antiferromagnetic configurations along with the average moment (μ_B/Ir).

Configurations	ΔE/Ir (meV)	Spin (Orb.) Moment/Ir
FM	0.0	0.43 (0.14)
AFM-a	-0.41	0.40 (0.16)
AFM-b	-0.24	0.40 (0.16)

order.

The onsite exchange energies corresponding to the TR odd multipole moments in the AFM2 state as a function of U are shown in Fig. 2(b) indicating no change in the hierarchy of the moments with U (see also Table II of SM). From Fig. 2(b), we gather that the spin moment is the POP for the system as it is associated with the highest onsite exchange energy (-120 meV for U=4 eV). This is in contrast to the case of SOC driven j_{eff}=1/2 Mott insulator Sr_2IrO_4[36] with a higher order multipole (Triakontadipole) as POP where spin and orbital moments are entangled.

Finally to check the possibility of a structural transition accompanied by a CO state, a complete structural relaxation calculation was performed (see SM). Calculations revealed environment of Ir-Ir dimer to be unaffected ruling out the possibility of a CO state very similar to $Ba_3M^{3+}Ru_2O_9$ systems[37].

Next we have analyzed the HP phase, considering a model structure (see SM), which has been described as a QSL state experimentally. In view of the large size of the unit cell all calculations for the HP phase have been done in the plane wave basis as implemented in the VASP code[5,6,11,12]. In Fig 3(c) we plot the total DOS for the paramagnetic phase in the presence of SOC and U. We find the system to be an insulator (for U_{eff}=U-J=1.5 eV) with an energy gap of 87 meV which is in agreement with the experiment[12]. In order to have an estimate of the intersite magnetic interaction in the HP phase, we have considered three magnetic configurations, namely FM, and two antiferromagnetic configurations AFM-a and AFM-b (see SM for description). The results of our calculation are shown in Table I. In sharp contrast to the AP phase the energy difference between the magnetic configurations are small (see Table I), implying the small energy scale of the intersite exchange interaction (J_{ex}) in the HP phase. The AFM configurations being lower in energy, indicate the presence of a weak AFM interaction in the system, consistent with the small value of θ_{CW} (=-1.6 K) obtained experimentally[12]. The weak J_{ex} due to disorder prohibits long range order in the HP phase.

It is quite clear from the above discussion that there is a competition between SOC and J_{ex} in the two phases of $Ba_3YIr_2O_9$. In the AP phase, while J_{ex} wins over SOC so that $\frac{J_{ex}}{\lambda} > 1$, the HP phase, on the other hand, has much weaker exchange interaction ($\sim$ few meV) compared to SOC (for iridates this is typically $\sim 10^2$ meV) making $\frac{J_{ex}}{\lambda} < 1$. The latter condition in the HP phase of $Ba_3YIr_2O_9$ is very similar to the spinel compound $FeSc_2S_4$[38]. Interestingly the model Hamiltonian considered for $FeSc_2S_4$ is also relevant for the cubic HP phase of $Ba_3YIr_2O_9$ as both of them have quite similar structure, therefore we expect in analogy, the stabilization of SOL state in the HP phase.

In conclusion, our detailed study of electronic and magnetic properties of $Ba_3YIr_2O_9$ both in the AP and HP phase suggest that a competition between J_{ex} and SOC decides the magnetic properties in both phases. In the AP phase the J_{ex} dominates over the SOC leading to long range magnetic order. The relatively weak value of SOC in the AP phase may be attributed to the large t_{2g} band width in $Ba_3YIr_2O_9$. The identification of the spin moment as the POP, also supports the fact that SOC is not so strong in the AP phase. In the HP cubic phase of $Ba_3YIr_2O_9$ the SOC dominates over the J_{ex} prohibiting long range order. Finally, we propose the pressure induced modulation of $\frac{J_{ex}}{\lambda} < 1$ in the HP phase is responsible for the SOL state.

Acknowledgments

The authors thank A. V. Mahajan, I. I. Mazin, and S. Streltsov for useful comments. I.D. thanks Department of Science and Technology (DST), Government of India for support. S.B. thanks Council of Scientific and Industrial Research (CSIR), India for a Fellowship. Y.L. and R.V. thank the Deutsche Forschungsgemeinschaft for financial support through grant TR/SFB 49. L.N. thanks Swedish Research Council (VR) for support.

* Presently at Uppsala University, Uppsala, Sweden
† sspid@iacs.res.in

[1] G. Cao, J. Bolivar, S. McCall, J. E. Crow, and R. P. Guertin, Phys. Rev. B **57**, R11039(R) (1998).
[2] R. Arita, J. Kunes, A. V. Kozhevnikov, A. G. Eguiluz, and M. Imada, Phys. Rev. Lett. **108**, 086403 (2012).
[3] Y. Singh and P. Gegenwart, Phys. Rev. B **82**, 064412 (2010).
[4] M. J. Lawler, A. Paramekanti, Y. B. Kim, and L. Balents, Phys. Rev. Lett. **101**, 197202 (2008).
[5] T. Dey, A. V. Mahajan, P. Khuntia, M. Baenitz, B. Koteswararao, and F. C. Chou, Phys. Rev. B **86**, 140405(R) (2012).
[6] A. Shitade, H. Katsura, J. Kunes, X.-L. Qi, S.-C. Zhang, and N. Nagaosa, Phys. Rev. Lett. **102**, 256403 (2009).
[7] H.-C. Jiang, Z.-C. Gu, X.-L. Qi, and S. Trebst, Phys. Rev. B **83**, 245104 (2011).
[8] S. K. Panda, S. Bhowal, A. Delin, O. Eriksson, and I.

Dasgupta, Phys. Rev. B **89**, 155102 (2014).
[9] B. J. Kim, H. Jin, S. J.Moon, J.-Y. Kim, B.-G. Park, C. S. Leem, Jaejun Yu, T. W. Noh, C. Kim, S.-J. Oh, J.-H. Park, V. Durairaj, G. Cao, and E. Rotenberg, Phys. Rev. Lett. **101**, 076402 (2008).
[10] B. J. Kim, H. Ohsumi, T. Komesu, S. Sakai, T.Morita, H. Takagi, and T. Arima, Science **323**, 1329 (2009).
[11] A. Nag *et. al*, arXiv:1506.04312v3.
[12] Tusharkanti Dey, A. V. Mahajan, R. Kumar, B. Koteswararao, F. C. Chou, A. A. Omrani, and H. M. Ronnow, Phys. Rev. B **88**, 134425 (2013).
[13] Simon A. J. Kimber, Mark S. Senn, Simone Fratini, Hua Wu, Adrian H. Hill, Pascal Manuel, J. Paul Attfield, Dimitri N. Argyriou, and Paul. F. Henry, Phys. Rev. Lett. **108**, 217205 (2012).
[14] Yoshihiro Doi and Yukio Hinatsu, J. Phys.: Condens. Matter **16** 2849 (2004).
[15] Tusharkanti Dey, R. Kumar, A. V. Mahajan, S. D. Kaushik, and V. Siruguri, Phys. Rev. B **89**, 205101 (2014).
[16] D. Singh and L. Nordström, Planewaves, Pseudopotentials, and the LAPW method (Springer, New York, 2006).
[17] F. Bultmark, F. Cricchio, O. Grånäs, and L. Nordström, Phys. Rev. B **80**, 035121 (2009).
[18] ELK is available at http://elk.sourceforge.net.
[19] J. P. Perdew, K. Burke, and M. Ernzerhof, Phys. Rev. Lett. **77**, 3865 (1996).
[20] P. Blaha, K. Schwarz, G. K. H. Madsen, D. Kvasnicka,J. Luitz, WIEN2k, *An Augmented Plane Wave + Local Orbitals Program for Calculating Crystal Properties* (Karlheinz Schwarz, Techn. Universiat Wien, Austria, 2001.
[21] P. E. Blöchl, Phys. Rev. B **50**, 17953 (1994).
[22] G. Kresse and D. Joubert, Phys. Rev. B **59**, 1758 (1999).
[23] G. Kresse and J. Hafner, Phys. Rev. B **47**, 558(R) (1993).
[24] G. Kresse and J. Furthmüller, Phys. Rev. B **54**, 11169 (1996).
[25] O. K. Andersen and T. Saha-Dasgupta, Phys. Rev. B **62**, R16219(R) (2000).
[26] O. K. Andersen, T. Saha-Dasgupta, R. W. Tank, C. Arcangeli, O. Jepsen, and G. Krier, Electronic Structure and Physical Properties of Solids. The Uses of the LMTO Method, Springer Lecture Notes in Physics (Berlin: Springer), 3 (2000).
[27] O. K. Andersen, T. Saha-Dasgupta, and S. Ezhov, Third-generation muffin-tin orbitals, Bull. Mater. Sci. **26**, 19 (2003).
[28] O. K. Andersen and O. Jepsen, Phys. Rev. Lett. **53**, 2571 (1984).
[29] Supplementary Materials for theoretical techniques.
[30] A. G. Petukhov, I. I. Mazin, L. Chioncel and A. I. Lichtenstein, Phys. Rev. B **67**, 153106 (2003).
[31] S.V. Streltsov, J. Terzic, J. C. Wang, Feng Ye, D.I. Khomskii, W. H. Song, S. J. Yuan, S. Aswartham, and G. Cao, arXiv:1505.00877.
[32] Soumyajit Sarkar, Molly De Raychaudhury, I. Dasgupta, and T. Saha-Dasgupta, Phys. Rev. B **80**, 201101(R) (2009).
[33] F. Cricchio, O. Grånäs, and L. Nordström, Eur. Phys. Lett. **94**, 57009 (2011).
[34] F. Cricchio, F. Bultmark, and L. Nordström, Phys. Rev. B **78**, 100404(R) (2008).
[35] F. Cricchio, F. Bultmark, O. Grånäs, and Lars Nordström, Phys. Rev. Lett. **103**, 107202 (2009).
[36] Shreemoyee Ganguly, Oscar Grånäs, and Lars Nordström, Phys. Rev. B **91**, 020404(R) (2015).
[37] Mark S. Senn, Simon A. J. Kimber, Angel M. Arevalo Lopez, Adrian H. Hill, and J. Paul Attfield, Phys. Rev. B **87**, 134402 (2013).
[38] Gang Chen, Leon Balents, and Andreas P. Schnyder, Phys. Rev. Lett. **102**, 096406 (2009); Gang Chen, Andreas P. Schnyder and Leon Balents, Phys. Rev. B **80**, 224409 (2009); S. Sarkar, T. Maitra, Roser Valentí, and T. Saha-Dasgupta, Phys. Rev. B **82**, 041105(R) (2010).

Supplementary Materials for Electronic Structure and Spin-orbit driven Magnetism in $d^{4.5}$ insulator $Ba_3YIr_2O_9$

I. COMPUTATIONAL DETAILS

Density functional theory calculations have been performed using four different methods, namely (a) (APW + lo)method as implemented in ELK, [1–3] (b)LAPW method as implemented in all electron full potential Wien2k code[4], (c) plane wave based method as implemented in Vienna *ab initio* simulation package (VASP) [5,6] and (d) N^{th} order muffin-tin orbital (NMTO) method[7–9]. In order to investigate the details of the physics for the hexagonal ambient pressure (AP) phase of $Ba_3YIr_2O_9$ we have performed calculations with the augmented plane waves plus local orbitals (APW + lo) method within the local density approximation (LDA) as well as LDA+U+SOC including successively the effect of SOC and Hubbard U as implemented in the code ELK.[1–3] The U parameter was expressed as a linear combination of Slater parameters, which in turn were calculated as the radial integrals of the Yukawa screened Coulomb potential, and the localized limit was adopted for the double counting correction.[2] A 10×10×6 k-mesh has been used for the Brillouin-Zone integration.
The calculations were also performed with generalized gradient correction (GGA) of Perdew-Burke-Ernzerhof [10] including Hubbard U and SOC as implemented in the all electron full potential Wien2k[4] code. We set the basis-size controlling parameter RK_{max} equal to 8 and considered a mesh of $9 \times 9 \times 3$ **k** points in the first Brillouin zone (FBZ) for the self-consistency cycle.

We have also used a plane wave based method as implemented in Vienna *ab-initio* simulation package (VASP)[5,6] where projector augmented wave potentials[11,12] are used to model the electron-ion interaction. A 10×10×6 k-mesh, similar to the ELK calculation, has been used for the Brillouin-Zone integration. Symmetry has been switched off in order to minimize possible numerical errors. In order to check, whether there is any structural transformation of the AP phase to charge ordered state, upon relaxation we have carried out relaxation calulations within the framework of GGA+U+SOC method. All structural relaxations were carried out until the Hellman-Feynman forces became less than 0.01 eV/A°. In this optimization, both the cell parameters and the positions of the atoms were allowed to relax. The experimentally synthesized HP cubic disordered structure is modelled by first constructing a 3×3×3 supercell of the ordered structure Ba_2YIrO_6 and then replacing 9 of the Y atoms by Ir atoms. In view of the large size of the unit cell the high pressure (HP) disordered cubic phase is studied only within GGA+U+SOC approach as implemented in VASP.
Finally to extract the tight binding parameters and to understand the crystal field splitting, we have constructed low energy model Hamiltonian using the downfolding procedure as implemented in the NMTO method.[7–9] The NMTO method, for which the selfconsistent version is yet to be available, relies on the selfconsistent potentials borrowed from the linear MTO (LMTO)[13] calculations. For the self-consistent LMTO calculations within the atomic sphere approximation (ASA), no empty sphere was used for $Ba_3YIr_2O_9$. For the space filling MT radii used for Ba, Y, Ir, and O were 2.28 Å, 1.50 Å, 1.30 Å, and 0.97 Å, respectively.

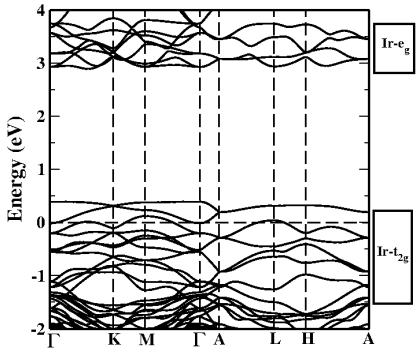

FIG. 4: LMTO Bandstructure of $Ba_3YIr_2O_9$ in absence of any magnetic order showing large t_{2g}-e_g splitting.

TABLE II: The hopping parameters (in meV) between the t_{2g} orbitals of the Ir atoms in the nonmagnetic phase of $Ba_3YIr_2O_9$.

Ir2	|1 >	|2 >	|3 >
Ir1 < 1|	-213.9	0.0	0.0
< 2|	0.0	-213.9	0.0
< 3|	0.0	0.0	-573.9

II. CRYSTAL FIELD SPLITTING AND ESTIMATION OF THE STRENGTH OF THE INTRA-DIMER HOPPING FOR $Ba_3YIr_2O_9$

In order to have a quantitative estimate of the intra dimer hopping strength and also to have an estimate of the various Ir d levels, we have carried out NMTO downfolding calculations for $Ba_3YIr_2O_9$ and constructed a Ir-d only low-energy Hamiltonian by integrating out the high energy degrees of freedom other than Ir-d. Diagonalization of the on-site block for $Ba_3YIr_2O_9$ gives the following five eigen states with energies -4.26, -4.26,-4.11, -0.48 and -0.48 eV respectively,

$$
\begin{aligned}
|1\rangle &= -0.8135|xy\rangle + 0.5815|yz\rangle \\
|2\rangle &= -0.5815|xz\rangle - 0.8135|x^2-y^2\rangle \\
|3\rangle &= |z^2\rangle \\
|4\rangle &= -0.5815|xy\rangle - 0.8135|yz\rangle \\
|5\rangle &= -0.8135|xz\rangle + 0.5815|x^2-y^2\rangle
\end{aligned}
$$

Clearly the first three states (|1 >, |2 >, and |3 >) form the t_{2g} manifold and the other two form the e_g manifold. From the calculated energy eigenvalues it is clear that the t_{2g} manifold splits into low lying doubly degenerate states |1 > and |2 > known as e_1 orbitals and singly degenerate state |3 > known as a_1 orbital. The t_{2g}-e_g crystal field splitting is quite large ($\sim$ 3.6eV) for $Ba_3YIr_2O_9$ which is also clear from Fig 4. We have displayed the intra-dimer hopping between the Ir t_{2g} states in Table II for $Ba_3YIr_2O_9$.

It is clear from Table II, that the direct hopping between the a_1 orbital is quite strong indicating the presence of strong intra dimer interaction in $Ba_3YIr_2O_9$.

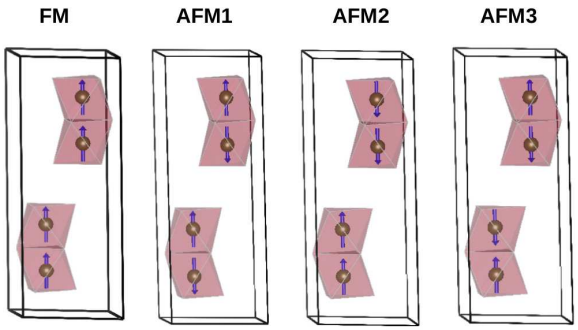

FIG. 5: Different magnetic configuration of $Ba_3YIr_2O_9$ in AP phase.

III. MAGNETIC CONFIGURATIONS

The total energy calculations are carried out for the ferromagnetic (FM) and three antiferromagnetic configurations namely AFM1, AFM2 and AFM3 for the AP phase of $Ba_3YIr_2O_9$. Fig 5 shows the spin structure corresponding to FM, AFM1, AFM2 and AFM3. The dominant TR odd multipole moments and onsite exchange energies associated with the AFM2 state are shown in Table III. For the HP phase of $Ba_3YIr_2O_9$ the total energy calculations are carried out for the magnetic configurations FM, AFM-a and AFM-b. Fig 6 shows the spin structure corresponding to these configurations. In the FM configuration all the spins on the 36 Ir atoms, present in the supercell, are aligned along (001)-axis, making all the Ir-Ir magnetic exchange interactions ferromagnetic. However AFM-a and AFM-b

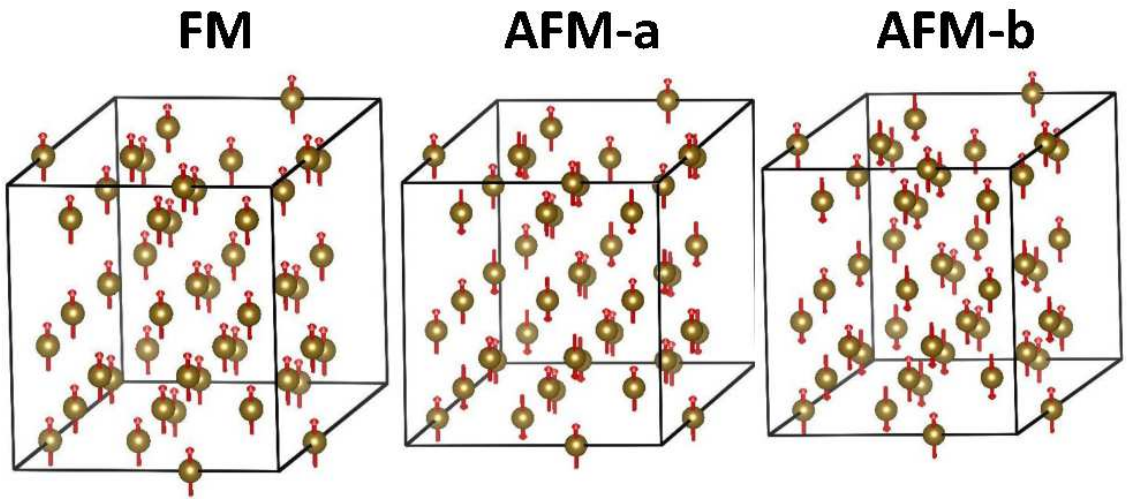

FIG. 6: Different magnetic configuration of $Ba_3YIr_2O_9$ in the HP phase

TABLE III: Study of the variation of band gap and Order Parameters (OP) with U for the AFM2 magnetic configuration. Significant magnetic OP like spin moment (w^{011}), orbital moment (w^{101}), triakontadipole moment (w^{415}) and octupole moment (w^{303}) are studied.

$\{U;J\}$ (in eV)	Band Gap (in meV)	w^{101} [Ex Eng] (in meV)	w^{011} [Ex Eng] (in meV)	w^{415} [Ex Eng] (in meV)	w^{303} [Ex Eng] (in meV)
$\{4;1\}$	252.42	0.34 [-10.0]	0.55 [-120]	1.96 [-36]	0.73 [-35]
$\{3;0.94\}$	73.05	0.30 [-6]	0.50 [-86]	1.77 [-22]	0.67 [-19]
$\{2.5;0.88\}$	0.0	0.26 [-3.78]	0.45 [-59.83]	1.55 [-14.49]	0.58 [-11.35]
$\{2;0.8\}$	0.0	0.02 [0.0]	0.04 [-0.5]	0.35 [-0.6]	0.06 [-0.09]

configurations are made in such a way that some of the Ir spins are pointed along (001)-axis while the rest are pointed along (00-1)-axis, which in turn make the presence of both ferromagnetic and antiferromagnetic Ir-Ir interactions in these two configurations as illustrated in Fig. 6. It is important to note that while the magnetic configurations are markedly different the energy difference between the magnetic configurations are small indicating a small energy scale of the intersite exchange interaction (see table-I in the main text).

* Presently at Uppsala University, Uppsala, Sweden
† sspid@iacs.res.in

[1] D. Singh and L. Nordström, Planewaves, Pseudopotentials, and the LAPW method (Springer, New York, 2006).
[2] F. Bultmark, F. Cricchio, O. Grånäs, and Lars Nordström, Phys. Rev. B **80**, 035121 (2009).
[3] ELK is available at http://elk.sourceforge.net.
[4] P. Blaha, K. Schwarz, G. K. H. Madsen, D. Kvasnicka,J. Luitz, WIEN2k, *An Augmented Plane Wave + Local Orbitals Program for Calculating Crystal Properties* (Karlheinz Schwarz, Techn. Universiat Wien, Austria, 2001.
[5] G. Kresse and J. Hafner, Phys. Rev. B **47**, 558 (1993).
[6] G. Kresse and J. Furthmller, Phys. Rev. B **54**, 11169 (1996).
[7] O. K. Andersen and T. Saha-Dasgupta, Phys. Rev. B 62, R16219. (2000).
[8] O. K. Andersen, T. Saha-Dasgupta, R. W. Tank, C. Arcangeli, O. Jepsen, and G. Krier, Electronic Structure and Physical Properties of Solids. The Uses of the LMTO Method, Springer Lecture Notes in Physics (Berlin: Springer) , 3 (2000).
[9] O. K. Andersen, T. Saha-Dasgupta, and S. Ezhov, Third-generation muffin-tin orbitals, Bull. Mater. Sci. 26, 19 (2003).
[10] J. P. Perdew, K. Burke, and M. Ernzerhof, Phys. Rev. Lett. **77**, 3865 (1996).

[11] P. E. Blöchl, Phys. Rev. B **50**, 17953 (1994).
[12] G. Kresse and D. Joubert, Phys. Rev. B **59**, 1758 (1999).
[13] O. K. Andersen and O. Jepsen, Phys. Rev. Lett. **53**, 2571 (1984).